The Astronomical Journal, 142, 109
Preprint typeset using LaTeX style emulateapj v. 11/10/09

IMPROVED MODELING OF THE MASS DISTRIBUTION OF DISK GALAXIES BY THE EINASTO HALO MODEL

Laurent Chemin[1,2], W. J. G. de Blok[3] and Gary A. Mamon[4]

The Astronomical Journal, 142, 109

ABSTRACT

The analysis of the rotation curves (RCs) of spiral galaxies provides an efficient diagnostic for studying the properties of dark matter halos and their relations with the baryonic material. Since the cored pseudo-isothermal (Iso) model usually provides a better description of observed RCs than does the cuspy NFW model, there have been concerns that the ΛCDM primordial density fluctuation spectrum may not be the correct one. We have modeled the RCs of galaxies from The HI Nearby Galaxy Survey (THINGS) with the Einasto halo model, which has emerged as the best-fitting model of the halos arising in dissipationless cosmological N-body simulations. We find that the RCs are significantly better fit with the Einasto halo than with either Iso or NFW halo models. In our best-fit Einasto models, the radius of density slope -2 and the density at this radius are highly correlated. The Einasto index, which controls the overall shape of the density profile, is near unity on average for intermediate and low mass halos. This is not in agreement with the predictions from ΛCDM simulations. The indices of the most massive halos are in rough agreement with those cosmological simulations and appear correlated with the halo virial mass. We find that a typical Einasto density profile declines more strongly in its outermost parts than any of the Iso or NFW models whereas it is relatively shallow in its innermost regions. The core nature of those regions of halos thus extends the cusp-core controversy found for the NFW model with low surface density galaxies to the Einasto halo with more massive galaxies like those of THINGS. The Einasto concentrations decrease as a function of halo mass, in agreement with trends seen in numerical simulations. However they are generally smaller than values expected for simulated Einasto halos. We thus find that the Einasto halo model provides, so far, the best match to the observed RCs, and can therefore be considered as a new standard model for dark matter halos.

Subject headings: cosmology: dark matter – galaxies: halos – galaxies: structure – galaxies: spiral – galaxies: kinematics and dynamics – galaxies: fundamental parameter

1. CONTEXT

One of the major tools in galactic dynamics is the decomposition of the rotation curves (hereafter, RCs) of spiral and lenticular galaxies into baryonic and dark components. This mass decomposition produces constraints on the distribution of dark matter in these galaxies, which permits the investigation of the possible relations between baryons and dark matter, and most importantly to study the properties of galactic dark matter halos.

Two spherical halo models are usually used for the mass decomposition of RCs. On one hand, cosmologists tend to favor the Navarro et al. (1996, hereafter, NFW) model

$$\rho_{\rm NFW}(r) = 4\,\rho_{-2}\,\frac{r_{-2}}{r}\,\left(\frac{r_{-2}}{r+r_{-2}}\right)^2\,, \qquad (1)$$

where r_{-2} is the radius where the density profile has a (logarithmic) slope of -2 (the "isothermal" value) and ρ_{-2} is the local density at that radius. The NFW model was originally thought (Navarro, Frenk & White 1997) to provide a universal description of halos of different mass produced in dissipationless (i.e. dark matter only) cosmological simulations run with different cosmologies, in particular in the Lambda Cold Dark Matter (hereafter, ΛCDM) paradigm. It has a cuspy inner structure with an inner slope of -1 and logarithmically diverges in mass at large radii. Note that steeper inner cusps (inner slopes as steep as $-3/2$) have been produced in other dissipationless cosmological simulations (Moore et al. 1999; Jing & Suto 2000; Diemand et al. 2004).

On the other hand, the analysis of RCs has traditionally used the so-called pseudo-isothermal (hereafter, Iso) model

$$\rho_{\rm Iso}(r) = 4\,\rho(a)\,\frac{a^2}{r^2+a^2}\,, \qquad (2)$$

which is often called the core halo because of its finite central density (but linearly diverging mass at large radii, where the asymptotic density slope is -2). This halo has no cosmological background but is often seen to better fit galactic RCs than the NFW model, particularly for dark matter dominated objects like low surface density galaxies (e.g. de Blok & Bosma 2002; Kuzio de Naray et al. 2006, 2008), for which the baryonic contribution can be largely neglected and the mass density profile as derived from the RC "directly" traces that of the dark matter halo. The disagreement between an observed, apparently finite, central density and the expectation of a steeper density profile from the ΛCDM cosmological simulations

chemin@obs.u-bordeaux1.fr, edeblok@ast.uct.ac.za, gam@iap.fr
[1] Université de Bordeaux, Observatoire Aquitain des Sciences de l'Univers, BP 89, 33271 Floirac Cedex, France
[2] CNRS, Laboratoire d'Astrophysique de Bordeaux-UMR 5804, BP 89, 33271 Floirac Cedex, France
[3] ACGC, Department of Astronomy, University of Cape Town, Rondebosch 7700, South Africa
[4] Institut d'Astrophysique de Paris (UMR 7095: CNRS & UPMC), 98 bis Bd. Arago, 75014 Paris, France

remains an unsolved problem in galactic dynamics (but see Governato et al. 2010). In fact, this *cusp-core controversy* has often been invoked as a major weakness of the current standard cosmological model of hierarchical growth of structures starting from a nearly homogeneous Universe, seeded with density fluctuations arising from a ΛCDM power spectrum. However, the impressive agreement between ΛCDM predictions and observations of the angular fluctuation spectrum of the Cosmic Microwave Background suggests that other explanations for the controversy must be sought, either in the dissipative and feedback physics of the baryons or in a more detailed analysis of halo density profiles from ΛCDM cosmological simulations.

Recently, Navarro et al. (2004) have proposed another model that fits the density profiles of halos in ΛCDM simulations even better than the NFW model. It was later realized (Merritt et al. 2006) that the model advocated by Navarro et al. (2004) had been previously introduced for the distribution of stellar light and mass in galaxies (Einasto 1965, 1968, 1969), with density profile

$$\rho_{\rm E}(r) = \rho_{-2}\ \exp\left\{-2n\ \left[\left(\frac{r}{r_{-2}}\right)^{1/n} - 1\right]\right\}\ , \quad (3)$$

where, again, r_{-2} is the radius where the density profile has a slope of -2 and ρ_{-2} is the local density at that radius. While both the NFW and Iso models are described by two parameters, a characteristic scale and a characteristic density at that radius, the Einasto model involves a third parameter, n, the Einasto index, which describes the shape of the density profile. The Einasto model is the three-dimensional equivalent of the Sérsic model (Sérsic 1968) that provides an excellent fit to the surface brightness profiles of elliptical galaxies (e.g. Kormendy et al. 2009).[5]

The mass profile of the Einasto halo (Cardone, Piedipalumbo & Tortora 2005; Mamon & Łokas 2005) is written as

$$M_{\rm E}(r) = 4\pi n r_{-2}^3 \rho_{-2}\ {\rm e}^{2n}\ (2n)^{-3n} \gamma\left(3n, \frac{r}{r_{-2}}\right), \quad (4)$$

where $\gamma(3n, x) = \int_0^x {\rm e}^{-t} t^{3n-1} dt$ is the incomplete gamma function.

As illustrated in Fig. 1 (top panel), the net effect of increasing the halo shape index n at fixed characteristic density and radius is to increase and steepen the density profile $\rho(r)$ in the central part of the halo. This then leads to increase the inner slope and amplitude of the RC (bottom panel of Fig. 1). Equation 4 also implies that an Einasto halo has a finite mass, whose physical feature is advantageous with respect to the divergent NFW and Iso mass profiles. At fixed characteristic Einasto scale density and radius, the mass profile converges more rapidly to its virial mass for small indices than for larger ones.

Because the inner RCs are expected to probe deeply inside the halos down to scales of 1/300th of the virial radius, where Navarro and co-workers have found small but significant departures between the density profiles of

[5] Both the NFW model (Łokas & Mamon 2001) and halos in ΛCDM simulations (Merritt et al. 2005) are well-fit by an $n = 3$ Sérsic model (Sérsic 1968).

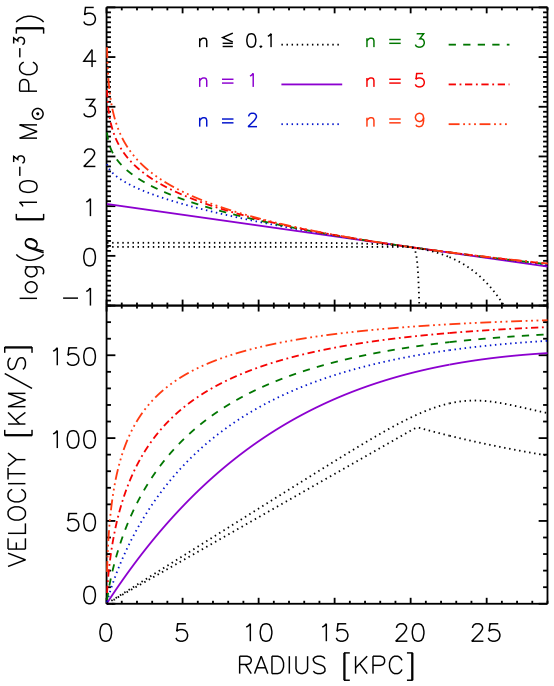

FIG. 1.— Density profile (*top*) and rotation curve (*bottom*) for Einasto models of different indices. The characteristic radius $r_{-2} = 20$ kpc and density $\rho_{-2} = 1.5 \times 10^{-3}\ \mathcal{M}_\odot\ {\rm pc}^{-3}$ are the same for all models. Only the Einasto index n changes as indicated by values and lines of various colour and style. The dotted black lines correspond to models with $n = 0.005$ (bottom curve) and $n = 0.1$ (upper curve).

ΛCDM halos and the NFW model, it has been suggested (e.g. Stoehr 2006) that the shallower inner slope of the Einasto model should reconcile the observed RCs with ΛCDM models. However, no extensive mass decompositions of galactic RCs using Einasto halos have yet been carried out. Only the RC of the Andromeda galaxy has been modeled with the Einasto formula (Chemin et al. 2009), though with no real improvement with respect to the usual core and NFW halos as caused by the peculiar shape of the M31 RC. Note also that Graham et al. (2006) compare the central dark matter densities of a sample of low surface brightness galaxies (de Blok 2004) to a family of Einasto halos and conclude that these match the data reasonably well.

The present article aims to provide the first mass decompositions of RCs with the Einasto model on an important sample of spiral galaxies. The questions we wish to address are the following. Is the Einasto halo a good fit to the RCs of galaxies? Is it a better description of observations than the usual NFW and Iso halos? What does a typical galactic Einasto halo look like?

We use a subsample from The HI Nearby Galaxy Survey (THINGS), as described in de Blok et al. (2008, hereafter D08) and in §2, and compare the quality of Einasto halo fits with those obtained using the NFW halo and pseudo-isothermal sphere (§3). We investigate the statistical significance of possible improvements of the Einasto model (§4), determine the parameter space of Einasto halos for the THINGS sample (§5) and compare the properties of galaxy-sized halos generated in numerical simulations to those derived from our sample

(§6). We also describe a range of Einasto indices (constrained two-parameter models) that provide better fits to RCs than the Iso and NFW models (§7). This article is intended to be the first in a series that aims at investigating how well the Einasto formalism works in galactic dynamics and at quantifying the degree of cuspiness of dark matter halos as a function of galaxy mass. The WMAP3 cosmology (Spergel et al. 2007) is adopted throughout this work.

2. THE THINGS SAMPLE

The HI observations of galaxies used in this study are from The HI Nearby Galaxy Survey (THINGS, Walter et al. 2008). This survey consists of high-resolution 21-cm observations of thirty-four nearby (closer than 15 Mpc) spiral and irregular galaxies (Sb to Im). The galaxies were observed with the Very Large Array (VLA) in its B, C, and D configurations. The HI data and the complete details of their reduction have been presented in previous articles from the THINGS series (see e.g. Walter et al. 2008). We analyze here the sample of seventeen rotationally dominated and undisturbed galaxies presented in D08, which is a subset of the whole sample from Walter et al. (2008).

3. MASS MODELING

3.1. *Generalities*

The reader is referred to D08 for the details of the kinematical analysis of the HI velocity fields by tilted ring models to extract the rotation curves. D08 has also presented a complete dynamical analysis of those RCs with the NFW and Iso models.

We have modeled the mass distribution using different RCs from those published in D08, as explained in §3.2. We have performed Levenberg-Marquardt non-linear least-squares fits to the RCs, taking into account the contributions of the gas, a spherical stellar bulge, a stellar disk, and a spherical dark matter component.

These contributions were taken from D08 for the stellar and gaseous RCs and from equation (4) for the halo. Basically the (atomic only) gaseous disk RCs come from THINGS HI surface densities and the stellar RCs from $3.6\,\mu m$ surface brightness profiles, available for all our galaxies from complementary observations with the *Spitzer* Nearby Galaxy Survey (SINGS, Kennicutt et al. 2003). The advantage of using these near-infrared luminosities, is that they are little affected by internal or Galactic extinction. We have not considered models with free mass-to-light ratios in combination with Einasto halos. Such an analysis will be presented in a future paper (Chemin et al., in preparation). Instead we have adopted the fixed mass-to-light ratios $\Upsilon_{3.6\mu m}$ of D08, who derived $\Upsilon_{3.6\mu m}$ from the 2MASS $J-K_s$ colors, adopting $\Upsilon_{3.6\mu m} = 0.92\,\Upsilon_{K_s} - 0.05$ (Oh et al. 2008), and $\log \Upsilon_{K_s} = 1.43\,(J-K_s) - 1.38$, extrapolated from Bell & de Jong (2001). Bell & de Jong (2001) derived stellar mass-to-light ratios assuming stellar populations with a bursty star formation history with a diet-Salpeter initial mass function (IMF). As in D08 we also consider the Kroupa (2001) IMF, which decreases the mass-to-light ratios (hence stellar masses) by 0.15 dex. A $\mathrm{sech}^2(z/z_0)$ law (van der Kruit & Searle 1981) was used to derive the vertical distribution of the stellar disk, under the hypothesis that the disk scale-height z_0 is one fifth the radial disk scale-length (van der Kruit & Searle 1981; Kregel et al. 2002).

None of our mass models take into account the contribution of molecular gas because the total gas surface densities are atomic gas dominated for the majority of our sample (Leroy et al. 2008). However we briefly report on the effects of molecular gas on Einasto halo parameters for the extreme case of NGC 6946 in §5.4.

Following D08 the RCs of the galaxies NGC 2403 and NGC 3198 have been decomposed using either one single stellar disk component (labeled "NGC2403d" and "NGC3198d") or two stellar components. Also, for NGC7793 we present the analysis of the whole RC, as well as that of its rising part only ("NGC7793s"). For each assumed IMF, fits have been performed using fixed and free Einasto indices for sake of comparison with cosmological simulations, as will be presented in Section 6. Further technical details of the fitting procedure are given in Chemin et al. (2009).

3.2. *The influence of RC sampling on mass models*

The RCs we fit here are sampled differently from those analyzed in D08, where the HI rotation velocities used for the dynamical analysis are not totally independent. D08 used a sampling of two data points per spatial resolution element. As a consequence they did not directly compare the χ^2 values obtained for the core and cusp models but instead studied the differences in χ^2.

Since a direct comparison of the reduced χ^2 values for the different two- and three-parameter models is essential to identify the "best" halo model, one has first to investigate whether any correlation between spatially adjacent rotation velocities could alter the results of the mass modeling. For this purpose, we have derived mass models of several galactic RCs from D08 and Chemin et al. (2009) using three different samplings, assuming Einasto, NFW and Iso halos.

A first modeling exercise (S1) was done with RCs sampled with two points per beam (as in D08), a second one (S2) with one point per beam (as in Chemin et al. 2009) and a third one (S3) with one point every two beams. The last two samplings provide independent data points, as opposed to the first one. The velocity uncertainties are defined as in D08 or Chemin et al. (2009), taking into account the (generally dominant) kinematical asymmetry observed between the receding the approaching halves of each galactic disk.

We observe the following results (which are strictly speaking only valid for the range of samplings explored here and should not be further generalized) : (i) the parameter space of the dark matter halo models does not vary with the spatial sampling of their RC, (ii) the relative fit quality of the three halo models does not vary with resolution, and (iii) the χ^2 values increase from S1 to S2 and then decrease for S3, which generally exhibits the smallest χ^2. To illustrate, the fits of the NFW, Iso and Einasto halos to the RC of the Andromeda galaxy lead to a reduced $\chi^2 \sim 7$ for S1 (sampling of $\sim$200 pc), $\chi^2 \sim 21$ for S2 (a sampling of $\sim$400 pc, as in Tab. 5 of Chemin et al. (2009), for their "hybrid" model) and $\chi^2 \sim 8$ for S3 (sampling of $\sim$800 pc). For this galaxy, the fit parameters of the NFW halo, the characteristic velocity v_{200} and the halo concentration c, are $v_{200} = (145 \pm 2)$

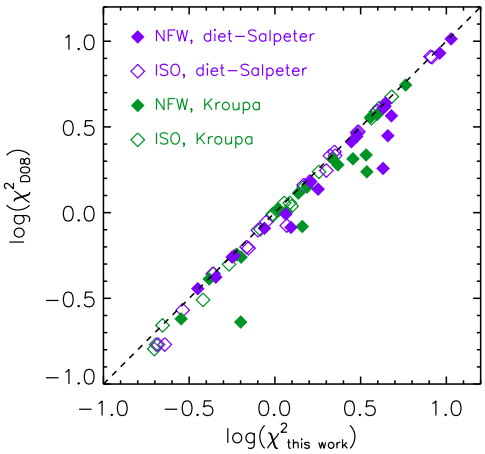

FIG. 2.— Comparison between reduced χ^2 from mass models fit to THINGS RCs from D08 and from this study, with the Iso (*Open diamonds*) and NFW (*closed diamonds*), using the Kroupa (*green*) and diet-Salpeter (*purple*) IMFs.

km s^{-1} and $c = 21 \pm 1$ for S1, $v_{200} = (146 \pm 4)$ km s^{-1} and $c = 20 \pm 2$ for S2, $v_{200} = (147 \pm 5)$ km s^{-1} and $c = 21 \pm 2$ for S3, indeed independent of the sampling.

The non-independent rotation velocities in S1 are thus responsible for the smaller χ^2 compared to S2, whereas the larger sampling interval explains the smaller χ^2 for model S3. The risk of using large intervals (like S3) is, of course, that one starts loosing small-scale details in the rotation curve and decreases the velocity gradient in the inner parts of the galaxies.

We therefore conclude that the optimum sampling of RCs for mass models of galaxies is one which avoids non-independent velocities generating artificially small χ^2, and which preserves an appropriate spatial resolution that does not smooth out small-scale details in the RC, especially in the inner regions, which are the most sensitive to the differences between the Iso, NFW and Einasto models. We have thus modeled the mass distributions of the THINGS galaxies from RCs with the S2 sampling, i.e., with galactocentric radii separated by one synthesized beam size.

Note that the conclusions given in D08 still hold: the halo parameters we have fit are similar to theirs, the Iso model usually provides better results than the NFW model. Only the values of the reduced χ^2 have increased when going from non-independent to independent velocities, as shown in Figure 2. Finally, because the analysis of individual differences between the NFW and Iso halos is beyond the scope of this article, we refer the reader to Tab. 1 and 2 for the resulting halo parameters and to D08 for further discussion.

3.3. *The Einasto model fits*

Figures 3 and 4 show the decomposition of the RCs into baryonic and dark matter components for the Einasto model. The fit parameters and their associated 1σ error, as well as the reduced chi-squared values, χ^2_r, are given in Tabs 1 and 2 for the Einasto, NFW and Iso halos. Figure 5 displays the values of Einasto χ^2_r and compares them with NFW and Iso χ^2_r values.

The most important results from the analysis of the fits are:

- The quality of the fits is very good for the majority of the galaxies. 80% (16 out of 20) of the fits done with a Kroupa IMF have $\chi^2_r < 1.5$. This fraction falls to 60% (12 out of 20) when using a diet-Salpeter IMF. The Einasto model is thus highly constrained (low χ^2) owing to the large numbers of degrees of freedom of each fit.

- Most of the fits (70%) with a Kroupa IMF are better (i.e., have lower χ^2_r) than those with a diet-Salpeter IMF. That trend is in good agreement with the results obtained for the NFW and Iso halos (see D08 and our current study in Tabs. 1 and 2). Both our analysis and that of D08 show how some mass models done under the prescriptions of Bell & de Jong (2001) with the assumption of a diet-Salpeter IMF can be unphysical due to modelled velocities exceeding observed ones in the inner disk regions (for, e.g., NGC 3521, NGC 5055, NGC 6946 or NGC 7331). It explains why the Einasto halo properties deduced from the diet-Salpter IMF often present scattered distributions and/or large errors, as will be shown in following sections. It is thus tempting to reject that IMF hypothesis. It is the reason why we focus more on the results obtained with the Kroupa IMF hypothesis hereafter, except where mentioned.

- The Einasto models give better results than the Iso and NFW models, irrespective of the IMF: 60% (80%) of the Einasto halos fit better than Iso halos for the diet-Salpeter IMF (Kroupa IMF, respectively); all of them fit better than the NFW cusp model, irrespective of the IMF. This result is expected owing to the effect of the third modeling parameter (the Einasto index) in addition to the usual characteristic scale halo density and size. We analyse the statistical significance of that modeling improvement in §4. Furthermore it is likely that the exponential-like decrease of the dark matter volumic density described by Eq. 3 contributes to the fit improvement as well, as will be shown in §7.

4. THE EINASTO MODEL AS THE PREFERRED MODEL

In this section, we investigate the significance of the improvement of the RC fits with the Einasto halo over those with the Iso and NFW models.

We first analyze the number of fits that are statistically significant with the Einasto model and that were not significant with any of the two-parameter Iso and NFW models. By "statistically significant" we mean that a model and the observations follow the same distribution, i.e., that there is less than 5% probability of obtaining as good a fit by chance according to chi-squared statistics. For the Kroupa IMF, the fraction of the fits that were not significant with the Iso model, but are with the Einasto halo consists of 30% of the sample (6 out of 20 fits). This fraction becomes 25% when going from NFW to Einasto. For the diet-Salpeter IMF, only two galaxies (10%) have gone from a not significant result with the Iso model to significant with the Einasto halo, while it is 20% from NFW to Einasto (4 galaxies).

Though these numbers do not represent the majority of the sample, they are not negligible. As a comparison,

TABLE 1
Fit parameters of the Einasto halo to THINGS galaxies for a free index and fixed mass-to-light ratios derived using a diet-Salpeter IMF.

Galaxy	EINASTO				NFW			Iso		
	χ^2_r	ρ_{-2} (10^{-3} $\mathcal{M}_\odot$ pc^{-3})	r_{-2} (kpc)	n	χ^2_r	v_{200} (km s^{-1})	c	χ^2_r	ρ_0 (10^{-3} $\mathcal{M}_\odot$ pc^{-3})	r_c (kpc)
	(1)	(2)	(3)	(4)	(5)	(6)	(7)	(8)	(9)	(10)
NGC925	1.2	3.4 ± 171.6	10.0 ± 1.1×10^3	10^{-3} ± 25.0	4.6	172.6 ± 17.6	1.3 ± 0.2	2.1	3.4 ± 0.8	16.8 ± 10.5
NGC2366	0.2	5.5 ± 1.2	3.2 ± 0.4	1.1 ± 0.2	1.2	71.2 ± 30.9	4.3 ± 2.3	0.2	37.6 ± 4.3	1.3 ± 0.1
NGC2403d	0.6	1.3 ± 0.3	17.1 ± 2.4	4.6 ± 0.5	0.6	109.7 ± 1.0	10.0 ± 0.2	0.9	81.8 ± 5.2	2.1 ± 0.1
NGC2403	0.6	1.6 ± 0.3	15.3 ± 1.8	4.1 ± 0.4	0.6	110.9 ± 1.5	9.8 ± 0.3	0.8	78.4 ± 4.7	2.1 ± 0.1
NGC2841	0.2	1.6 ± 0.5	28.5 ± 5.0	10.4 ± 1.6	0.5	182.8 ± 1.7	16.4 ± 0.3	0.3	298.0 ± 21.5	2.0 ± 0.1
NGC2903	0.3	36.5 ± 5.5	4.3 ± 0.4	8.2 ± 1.6	0.4	112.2 ± 0.8	31.5 ± 0.8	0.7	> 1000	0.0 ± 0.1
NGC2976	2.1	10.1 ± 3.3×10^6	8.0 ± 6.6×10^7	0.1 ± 2×10^5	3.0	62.1 ± 12.7	1.8 ± 0.4	2.0	11.6 ± 4.6	10.6 ± 54.9
NGC3031	2.6	7.0 ± 1.7	7.7 ± 0.9	0.1 ± 0.2	4.4	184.0 ± 161.0	3.2 ± 3.2	4.0	14.7 ± 6.0	5.3 ± 2.0
NGC3198d	1.2	1.2 ± 0.2	17.2 ± 1.2	1.5 ± 0.3	1.8	122.8 ± 5.6	5.2 ± 0.5	1.2	15.1 ± 2.2	4.9 ± 0.4
NGC3198	2.3	1.2 ± 0.3	17.0 ± 1.5	1.4 ± 0.4	3.0	122.1 ± 7.1	5.2 ± 0.7	2.2	14.4 ± 2.8	5.0 ± 0.6
IC2574	0.2	0.7 ± 0.4	15.8 ± 6.9	1.0 ± 0.4	4.3	69.3 ± 5.8	3.4 ± 0.1	0.2	4.0 ± 0.2	7.4 ± 0.5
NGC3521	8.4	0.7 ± 3.8	28.6 ± 114.0	0.3 ± 3.4	9.1	89.5 ± 155.9	2.1 ± 7.2	8.2	1.3 ± 1.8	36.3 ± 107.4
NGC3621	0.7	0.6 ± 0.3	27.2 ± 6.7	2.6 ± 0.6	0.9	168.8 ± 7.3	3.7 ± 0.2	0.7	14.4 ± 0.9	5.6 ± 0.2
NGC4736	1.2	5.5 ± 7.4	5.4 ± 16.8	10^{-3} ± 0.7	1.6	39.5 ± 16.5	7.9 ± 7.9	1.6	17.0 ± 28.4	1.8 ± 1.9
DDO154	0.3	1.4 ± 0.3	6.0 ± 0.8	2.2 ± 0.3	1.2	63.8 ± 2.6	4.1 ± 0.1	0.4	27.6 ± 2.4	1.3 ± 0.1
NGC5055	7.7	0.7 ± 0.2	32.2 ± 4.3	0.1 ± 0.2	10.7	234.6 ± 26.1	0.9 ± 0.1	8.1	0.9 ± 0.3	44.7 ± 30.2
NGC6946	1.3	4.6 ± 2.9	14.9 ± 8.3	2×10^{-3} ± 0.3	2.8	307.4 ± 37.5	1.9 ± 0.3	1.5	5.3 ± 0.5	21.4 ± 5.8
NGC7331	3.1	1.0 ± 4.8×10^5	> 1000	0.2 ± 3×10^5	4.3	275.0 ± 131.7	1.1 ± 0.9	3.0	1.6 ± 0.4	113.3 ± 519.4
NGC7793	1.7	22.7 ± 1.9	3.7 ± 0.1	0.3 ± 0.1	4.4	141.4 ± 8.1	6.6 ± 0.2	3.1	78.2 ± 11.2	1.9 ± 0.2
NGC7793s	1.5	< 10^{-3}	> 1000	9.3 ± 42.3	4.8	181.0 ± 20.8	5.6 ± 0.4	2.2	51.8 ± 6.8	3.5 ± 0.7

Note. — Columns (1)-(5)-(8) Reduced χ^2. Columns (2)-(9) Characteristic density. Columns (3)-(10) Characteristic radius. Column (4) Einasto index. Columns (6)-(7) NFW halo characteristic velocity and concentration.

TABLE 2
Same as in Tab. 1 but with mass-to-light ratios derived using a Kroupa IMF.

Galaxy	EINASTO				NFW			Iso		
	χ^2_r	ρ_{-2} (10^{-3} $\mathcal{M}_\odot$ pc^{-3})	r_{-2} (kpc)	n	χ^2_r	v_{200} (km s^{-1})	c	χ^2_r	ρ_0 (10^{-3} $\mathcal{M}_\odot$ pc^{-3})	r_c (kpc)
NGC925	0.6	4.5 ± 0.5	8.9 ± 0.6	0.1 ± 0.1	3.4	171.4 ± 15.2	2.2 ± 0.1	1.1	6.0 ± 0.8	9.6 ± 1.8
NGC2366	0.2	5.7 ± 1.1	3.2 ± 0.3	1.1 ± 0.2	1.2	75.4 ± 16.3	4.2 ± 0.8	0.2	40.1 ± 4.2	1.3 ± 0.1
NGC2403d	0.6	1.5 ± 0.4	15.6 ± 2.0	5.6 ± 0.5	0.6	101.2 ± 1.0	12.6 ± 0.3	1.1	154.0 ± 10.8	1.5 ± 0.1
NGC2403	0.6	1.7 ± 0.4	14.6 ± 1.8	5.3 ± 0.5	0.6	102.0 ± 0.9	12.4 ± 0.2	1.0	147.0 ± 9.9	1.5 ± 0.1
NGC2841	0.2	10.7 ± 1.2	11.2 ± 0.6	12.4 ± 1.5	0.6	172.0 ± 1.4	25.2 ± 0.6	0.2	> 1000	0.6 ± 0.1
NGC2903	0.3	72.4 ± 19.4	3.2 ± 0.4	9.6 ± 2.1	0.4	111.2 ± 0.8	36.2 ± 1.0	1.2	> 1000	0.0 ± 0.1
NGC2976	0.5	0.0 ± 0.6	> 1000	4.9 ± 77.8	2.3	108.6 ± 5.9	4.5 ± 0.2	0.5	36.6 ± 4.7	4.5 ± 2.8
NGC3031	3.1	30.0 ± 3.0	4.7 ± 0.2	0.7 ± 0.2	3.6	94.3 ± 5.5	26.8 ± 3.6	3.9	740.0 ± 434.0	0.8 ± 0.3
NGC3198d	0.8	2.2 ± 0.2	13.1 ± 0.6	2.1 ± 0.3	1.4	109.3 ± 2.5	8.9 ± 0.6	0.8	47.1 ± 5.9	2.7 ± 0.2
NGC3198	1.5	2.2 ± 0.3	13.0 ± 0.7	2.0 ± 0.3	2.2	109.9 ± 3.2	8.7 ± 0.7	1.5	44.3 ± 7.4	2.8 ± 0.3
IC2574	0.2	0.7 ± 0.3	15.1 ± 5.0	1.1 ± 0.3	3.4	94.6 ± 4.3	2.2 ± 0.2	0.2	4.9 ± 0.2	6.3 ± 0.3
NGC3521	4.9	6.1 ± 2.5	9.4 ± 1.6	1.2 ± 0.9	5.8	121.7 ± 22.1	9.7 ± 3.1	4.8	75.6 ± 45.8	2.5 ± 0.9
NGC3621	0.6	0.3 ± 0.2	39.9 ± 12.3	6.4 ± 1.0	0.6	119.8 ± 1.9	7.9 ± 0.3	1.3	49.3 ± 4.2	2.8 ± 0.1
NGC4736	1.5	50.8 ± 15.5	1.8 ± 0.3	1.9 ± 0.8	1.5	44.1 ± 2.3	43.8 ± 9.0	1.8	> 1000	0.1 ± 0.1
DDO154	0.3	1.5 ± 0.3	5.9 ± 0.8	2.2 ± 0.3	1.4	91.3 ± 4.0	2.7 ± 0.1	0.4	28.5 ± 2.5	1.3 ± 0.1
NGC5055	0.8	1.3 ± 0.1	22.6 ± 0.6	0.5 ± 0.1	1.6	234.4 ± 22.5	1.9 ± 0.3	1.0	4.8 ± 0.5	11.7 ± 0.9
NGC6946	1.0	1.8 ± 1.2	18.7 ± 7.4	2.6 ± 0.9	1.0	187.9 ± 17.0	6.1 ± 0.7	1.0	44.2 ± 4.1	3.7 ± 0.2
NGC7331	0.3	0.0 ± 0.0	> 1000	13.1 ± 19.7	0.3	195.6 ± 15.3	5.2 ± 0.6	0.4	26.1 ± 3.6	5.2 ± 0.5
NGC7793	2.8	19.8 ± 3.7	3.6 ± 0.3	0.9 ± 0.2	3.9	114.4 ± 10.2	9.2 ± 0.8	3.7	128.0 ± 17.6	1.5 ± 0.1
NGC7793s	1.7	< 10^{-3}	> 1000	12.7 ± 32.9	2.9	191.9 ± 9.7	6.1 ± 0.4	4.1	96.7 ± 15.1	2.0 ± 0.3

15% (20%) of the sample acquires significant fits when passing from NFW to Iso for the Kroupa (respectively diet-Salpeter) IMF. Therefore, the improvement of fitting the HI RCs by the Einasto model instead of the Iso or NFW models is equal to or better than the improvement implied when switching from NFW to Iso. Conversely, the Einasto model does not diminish the significance of the fits : no fit has turned from being significant with Iso/NFW to not significant with the Einasto halo, regardless of the IMF.

However, it is not surprising that the three-parameter Einasto model is better able to reproduce the RCs than the two-parameter Iso and NFW models. Because neither Iso nor NFW models are nested[6] into the Einasto family of models, we cannot simply perform an F-test to check for the significance of the improvement of the fits with the three-parameter Einasto model. Instead, we verify the significance of this improvement by performing Akaike information criterion tests (hereafter, AIC, Akaike 1974), which are designed to compare non-nested

[6] A model with k parameters is considered nested in a more complex model with e.g., $k+1$ parameters when fixing one of the $k+1$ parameters allows one to reproduce the simplest k parameter model.

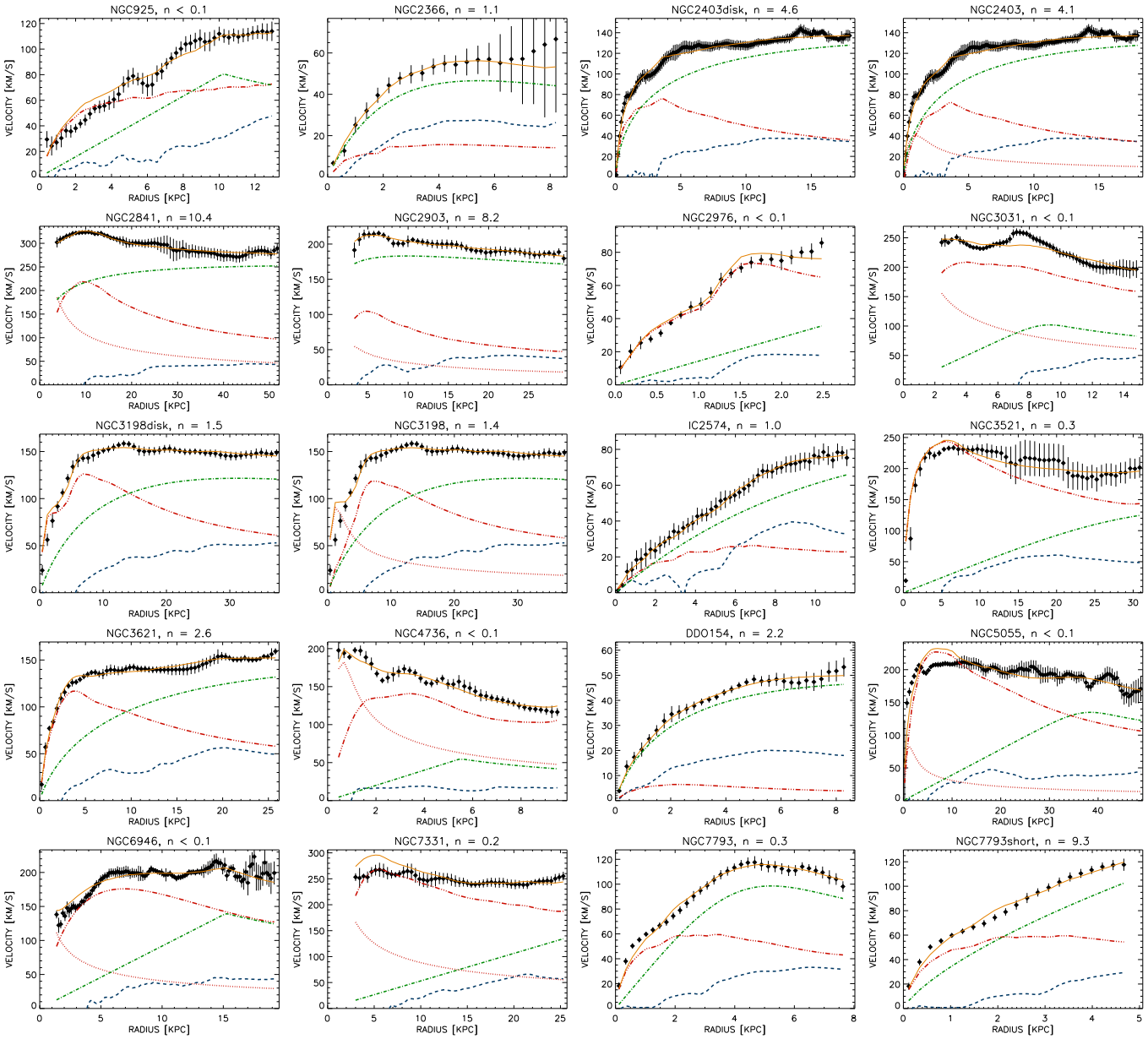

FIG. 3.— Mass models for the Einasto halo derived from the HI RC of THINGS galaxies. Displayed results are for fixed stellar mass-to-light ratios derived from stellar population synthesis with a diet-Salpeter initial mass function and whose values are given in D08. A red dashed-dotted (dotted) line is for the stellar disk (bulge, respectively) components, a blue dashed line for the atomic gas, a green dashed-dotted line for the dark halo and an orange thick line for the overall model.

models of different numbers of parameters. The goal of an AIC test is not to statistically reject one model with respect to another, but rather to find the model that is more likely to be correct. The criterion is expressed as AIC $= \chi^2 + 2N$, where N is the number of parameters of the model. An Einasto model is considered more likely to be correct than the Iso or NFW model when $\mathrm{AIC_{Einasto}} < \mathrm{AIC_{Iso/NFW}}$. We find that 65% (60%) of the fits with the Einasto model are more likely to be correct than those with the ISO model assuming a Kroupa (diet-Salpeter) IMF. These percentages increase to 95% when comparing with the NFW model, independent of the assumed IMF.

In summary, the Einasto model provides more fits that are statistically significant and is more likely to be correct than the two other models. For these reasons, we conclude that fitting RCs of the current THINGS sample with an Einasto halo is a significant improvement with respect to the NFW and Iso models.

5. DYNAMICAL PROPERTIES OF EINASTO HALOS

5.1. *Non-universality of the halo*

Figures 6 and 7 show the fit parameters for the diet-Salpeter and Kroupa IMFs, respectively. Figure 8 shows the distribution of Einasto indices. Based on these distributions, we can distinguish several families of halos. A first family of halos has well constrained parameters with large indices ($n > 4$). We refer to this family as cuspy Einasto halos hereafter. Indeed it corresponds to halos whose indices are comparable with the index of

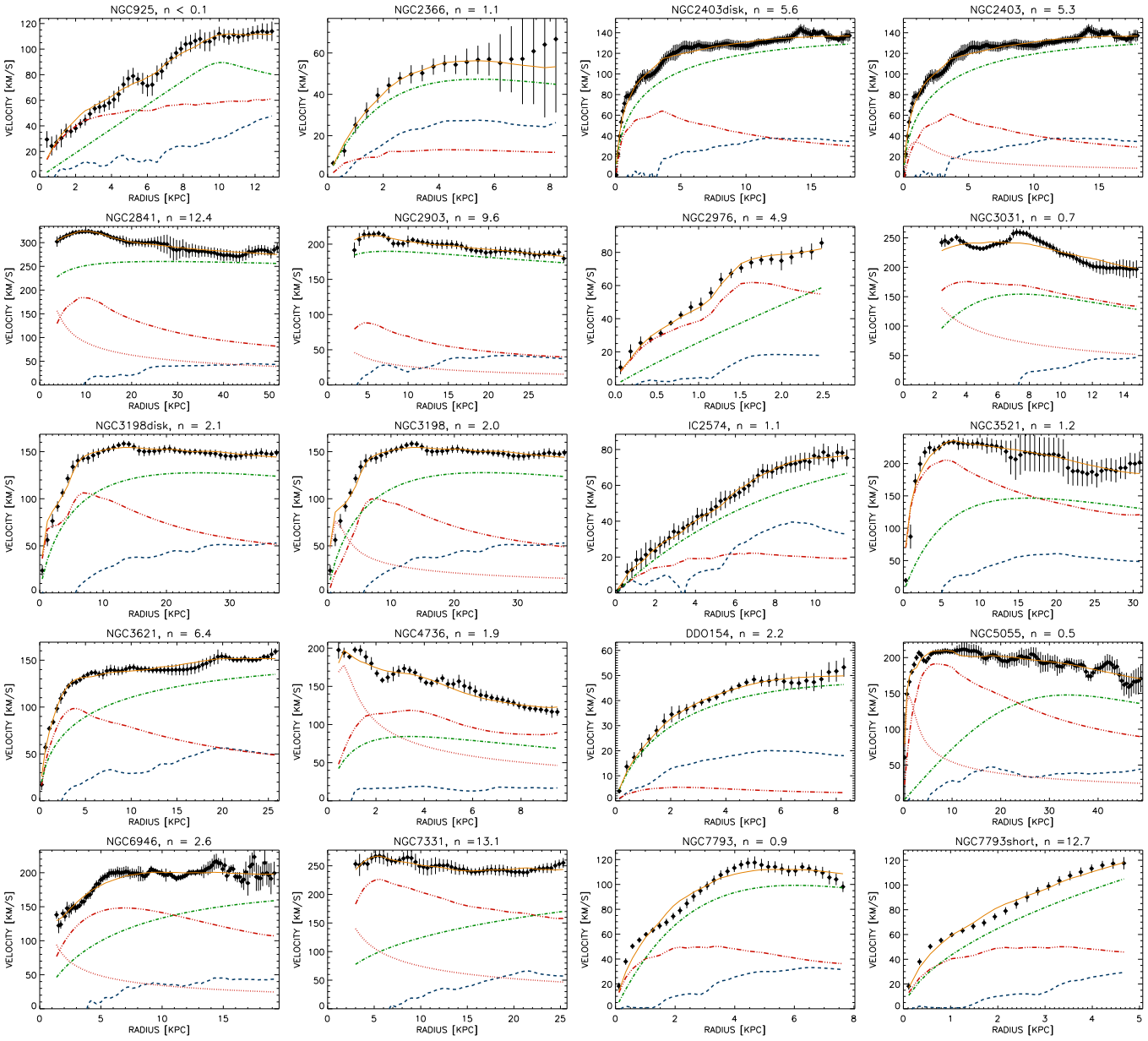

FIG. 4.— Same as Fig. 3 but with a Kroupa initial mass function.

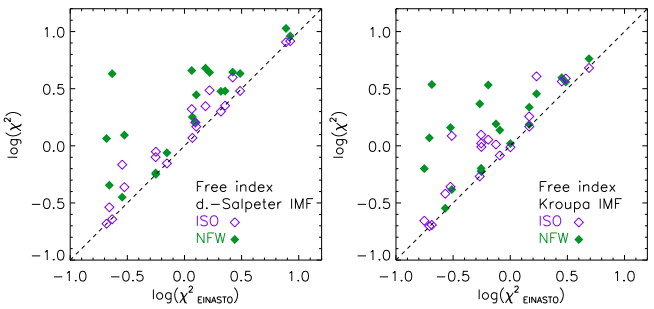

FIG. 5.— Comparison of reduced χ^2 for the Einasto halo with the NFW and Iso halos (respectively filled and open symbols), using the diet-Salpeter (*left*) and Kroupa (*right*) IMFs.

a typical galaxy-sized halo from numerical simulations ($5 \leq n_{\rm simulated} \leq 7$, Navarro et al. 2004; Merritt et al. 2006; Graham et al. 2006; Navarro et al. 2010). Their innermost density slopes are steeper than -0.8, hence consistent with cosmological slopes ($\alpha = -0.9 \pm 0.1$, Navarro et al. 2010). A second family of galaxies has well-constrained parameters with low index values ($0.1 < n \leq 4$). It contains the majority of the galaxies. A third halo family has very low indices ($n \leq 0.1$). Most of those fits occur with the diet-Salpeter IMF. Finally a fourth family of halos has unrealistic, extremely large scale radii, with large associated uncertainties (the rising part of the RC of NGC 7793, NGC 7331, NGC 2976). Those fits are extremely degenerate, which is very likely caused by an almost complete dominance of the baryonic material over the dark component, at least for NGC 2976 and NGC 7331.

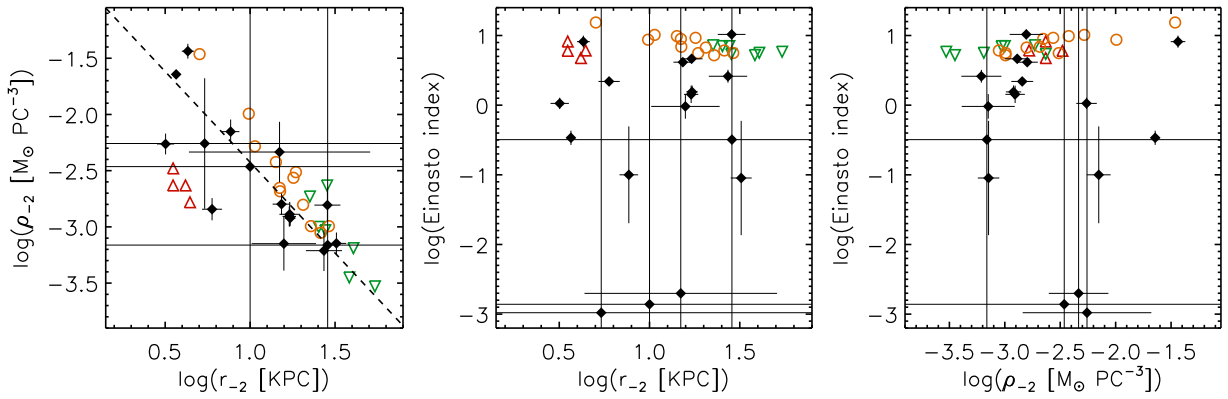

FIG. 6.— Parameter space $[\rho_{-2}, r_{-2}, n]$ of Einasto halos for the THINGS sample (filled diamonds). Fixed stellar mass-to-light ratios are derived from stellar population synthesis using a diet-Salpeter initial mass function. Colored symbols show the parameters of dwarf- (upward red triangles) and galaxy- (downward green triangles) halos modeled in ΛCDM simulations (Navarro et al. 2004). Galaxy-sized halos from Tissera et al. (2010) are displayed with orange circles. A dashed line is a power law fit to the relationship linking ρ_{-2} and r_{-2}: $\log(\rho_{-2}) = (-1.61 \pm 0.07)\log(r_{-2}) - (0.81 \pm 0.06)$. The degenerate fits with $\log r_{-2} > 3$ and $\log \rho_{-2} > -5$ are not drawn for clarity.

Figures 6 and 7 show a clear relation linking the characteristic density to the radius. Small halos are denser than large ones. A power-law fit to the observed relationship gives $\rho_{-2} \propto r_{-2}^{-1.6\pm0.1}$ for both IMFs. This implies that the surface density of dark matter $\Sigma_{-2} = \rho_{-2} r_{-2}$ derived at r_{-2} scales as $\Sigma_{-2} \propto r_{-2}^{-0.6} \propto \rho_{-2}^{3/8}$. Those relations have been determined without taking account the fourth halo family fits and by averaging the fit parameters of galaxies that have duplicated RCs but a different stellar decomposition (NGC 2403 and NGC 3198). It is worthwhile to note that the correlation we find between the scale density and radius of the Einasto model differs from the relations found between the scale density and radius of two-parameter NFW and Iso models. For instance Kormendy & Freeman (2004) and Spano et al. (2008) have derived a relation $\rho_0 \propto 1/r_0$ (but see Barnes et al. 2004), where the scale density ρ_0 and and r_0 are the characteristic density and radius of two-parameter NFW and Iso models. As a consequence the dark matter surface density $\Sigma_0 = \rho_0 r_0$ remains roughly constant at the core radius of the halo (Kormendy & Freeman 2004; Spano et al. 2008; Donato et al. 2009). This trend is not observed with the Einasto halo. In this context, it is interesting to note that we have also fit the two-parameter Iso model to the current sample (Iso column in Tabs. 1 and 2). The results do not imply a similar relation as in Kormendy & Freeman (2004), Spano et al. (2008) or Donato et al. (2009), but agree more with Barnes et al. (2004). We indeed find inner surface densities for the core halo that depend on the scale parameters. A linear fit yields $\rho_0 \propto r_0^{-1.4\pm0.03}$ for the diet-Salpeter IMF and $\rho_0 \propto r_0^{-1.5\pm0.04}$ for the Kroupa IMF. It may seem odd that these results disagree with Donato et al. (2009) because part of their sample consists of the current THINGS galaxies (though using the D08 RCs). A possible explanation of the difference could be the choice of stellar mass-to-light ratios (Donato et al. use best fit mass-to-light ratios), the use of other kinematical tracers (mostly the ionized gas) as well as the choice of the outer slope of the density profile of dark matter ($\rho \propto r^{-3}$ in Spano et al. and Donato et al., while our Iso model implies $\rho \propto r^{-2}$). A detailed investigation of both analysis methods is beyond the scope of this article. Clearly though, the implied (non-)constancy of the dark matter surface density warrants further investigation.

As for the Einasto index, we note the more scattered distribution and the presence of more halos having a small index for the diet-Salpeter IMF than for the Kroupa IMF. This is caused by a larger contribution of stellar baryons to the RCs. The effect of a (very) low index (illustrated in Fig. 1 as declining velocities in the outer parts of the dark matter halo) are clearly visible for NGC 4736, NGC 6946 (Fig. 3, diet-Salpeter IMF only) and NGC 925 (Figs. 3 and 4).

No obvious correlation is found between the Einasto index and scale density or radius. Using halos with $n \leq 4$ (second and third halo families) we derive an average index of $\bar{n} = 0.8 \pm 0.3$ with the diet-Salpeter IMF and $\bar{n} = 1.3 \pm 0.2$ with the Kroupa IMF (using averaged indices for NGC 2403/NGC 2403d and NGC 3198/NGC 3198d). Note that the amplitude and scatter become more important if the first halo family is also taken into account, with $\bar{n} = 2.1 \pm 0.8$ (diet-Salpeter) and $\bar{n} = 3.2 \pm 0.9$ (Kroupa).

The cuspiest Einasto halos are typically found in galaxies where the dark matter dominates the visible matter at almost all radii (as seen in Figs. 3 and 4), coupled with a relatively extended rotation curve and mass distribution ($r > 15$ kpc) with rotation velocities larger than 120 km s^{-1} at large galactocentric radius. Note also they correspond to galaxies whose RCs start at $r \geq 3$ kpc. The missing information at $r < 3$ kpc might affect our conclusions for those galaxies.

Perhaps the most important result from the analysis of the indices is that no single value or well-defined relation can reproduce all types of halos. The index is also a complex function of the halo mass (see §5.3). We can thus conclude that no obvious "universal" Einasto index, hence Einasto halo, can be deduced from the current galaxy sample.

5.2. *Intermediate class halo density and density slope profiles*

Figure 9 displays the radial profiles of the mass volume density and the radial profiles of the logarithmic

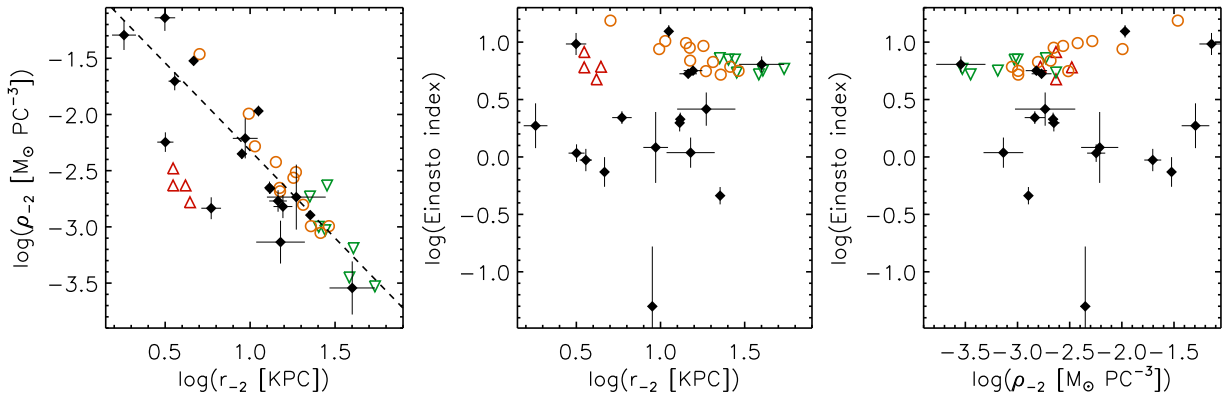

FIG. 7.— Same as Figure 6 but for a Kroupa initial mass function. The dashed line is a power law fit $\log(\rho_{-2}) = (-1.56 \pm 0.06)\log(r_{-2}) - (0.76 \pm 0.06)$.

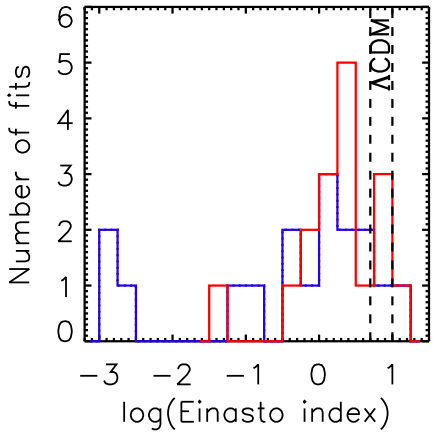

FIG. 8.— Distribution of Einasto indices. Results for the diet-Salpeter and Kroupa IMFs are shown by blue and red histograms, respectively. The range of Einasto indices from ΛCDM simulations with and without the physics of baryons ($5 \lesssim n \lesssim 10$) is displayed by dashed lines.

density slope of the THINGS sample. For clarity, only results for the Kroupa IMF are represented, excluding the fourth halo family. Our conclusions are similar for the diet-Salpeter IMF. Also shown are the radial profiles of generic galaxy-sized Iso and NFW halos with comparable densities, giving a halo RC with a velocity amplitude of ~ 200 km s^{-1} at a typical radius of 25 kpc. Other dashed colored curves correspond to Einasto halos with parameters derived from cosmological simulations (see §6 for details).

Figure 9 (top panel) shows that the density profiles typically decrease very smoothly in the inner regions. Further out, the profiles become very steep and the densities very low past the scale radius r_{-2}. It can also be seen that most of the halos derived from the observations are less dense in their inner parts than any of the simulated galaxy-sized halos. All of this is explained by the fact that THINGS galaxies generally have small Einasto indices whereas simulated halos have large index values due to their cuspy nature (see §6 for a complete discussion).

The bottom panel of Fig. 9 shows that on the one hand, the logarithmic slopes in the innermost regions are more reminiscent of the slope of a Iso halo than that of cosmological Einasto or NFW cusps, for the majority of the sample. On the other hand, because of the progressively steepening nature implied by the Einasto model (Eq. 3), the observed slope profiles become similar to a NFW cusp at larger radii. The slopes are even larger than those of any cosmological halos beyond r_{-2}, as a result of the small amplitude of the observed Einasto indices. A density slope profile of a typical observed Einasto halo ($\log(\rho_{-2}\ \mathcal{M}_\odot \mathrm{pc}^{-3}) \sim -2$, $r_{-2} \sim 10$ kpc, $n \sim 1.3$, as fit with the Kroupa IMF) thus represents an intermediate case between a pseudo-isothermal core halo and cosmological cusps inside r_{-2}. As a consequence of these results, we estimate that half of the total mass of such halos is contained within about 15 kpc, and the mass profile has rapidly converged towards, e.g. 95% its total mass at $r \sim 40$ kpc only (or four times the average scale radius r_{-2}).

We report the inner slopes $\alpha = \mathrm{d}\log(\rho)/\mathrm{d}\log(\mathrm{r})$ of the dark matter density profiles in Tab. 3. For sake of uniformity with cosmological simulations whose inner slopes are derived at a fraction of the Einasto radius r_{-2} (basically $-2 < \log(r/r_{-2}) < -1$, Navarro et al. 2010), we have derived the inner slopes of the THINGS sample at $\log(r/r_{-2}) = -1.5$ (or $r = 0.03 r_{-2}$), discarding all fits of the fourth halo family. The mean logarithmic slope of the density profiles is $\bar{\alpha} = -0.3 \pm 0.1$ for the diet-Salpeter IMF and $\bar{\alpha} = -0.5 \pm 0.1$ for the Kroupa IMF. Those

TABLE 3
LOGARITHMIC SLOPE α OF THE DARK MATTER DENSITY PROFILE DERIVED AT $\log(r/r_{-2}) = -1.5$.

Galaxy	α (diet-Salpeter IMF)	α (Kroupa IMF)
NGC925	$\lesssim 0 \pm 0.01$	$\lesssim 0 \pm 0.01$
NGC2366	-0.08 ± 0.01	-0.08 ± 0.01
NGC2403	-0.91 ± 0.03	-1.06 ± 0.03
NGC2841	-1.43 ± 0.03	-1.51 ± 0.01
NGC2903	-1.31 ± 0.01	-1.40 ± 0.02
NGC3031	$\lesssim 0 \pm 0.01$	-0.02 ± 0.01
NGC3198	-0.20 ± 0.01	-0.37 ± 0.01
IC2574	-0.05 ± 0.03	-0.08 ± 0.03
NGC3521	$\lesssim 0 \pm 0.01$	-0.12 ± 0.02
NGC3621	-0.53 ± 0.05	-1.17 ± 0.07
NGC4736	$\lesssim 0 \pm 0.01$	-0.32 ± 0.03
DDO154	-0.41 ± 0.03	-0.42 ± 0.03
NGC5055	$\lesssim 0 \pm 0.01$	$\lesssim 0 \pm 0.01$
NGC6946	$\lesssim 0 \pm 0.01$	-0.53 ± 0.09
NGC7793	$\lesssim 0 \pm 0.01$	-0.05 ± 0.01

numbers become $\bar{\alpha} = -0.1 \pm 0.1$ and $\bar{\alpha} = -0.2 \pm 0.1$ (respectively) when the cuspiest halos of the sample ($n > 4$) are removed from the distribution. Note that the mean inner density slope is -1.3 ± 0.2 for those cuspiest halos only. For comparison, the innermost slope in the Aquarius pure-ΛCDM simulation (at $r_{-2}/100$) is -0.9 ± 0.1, which is shallower than the cuspiest of our halos, but steeper than most of them.

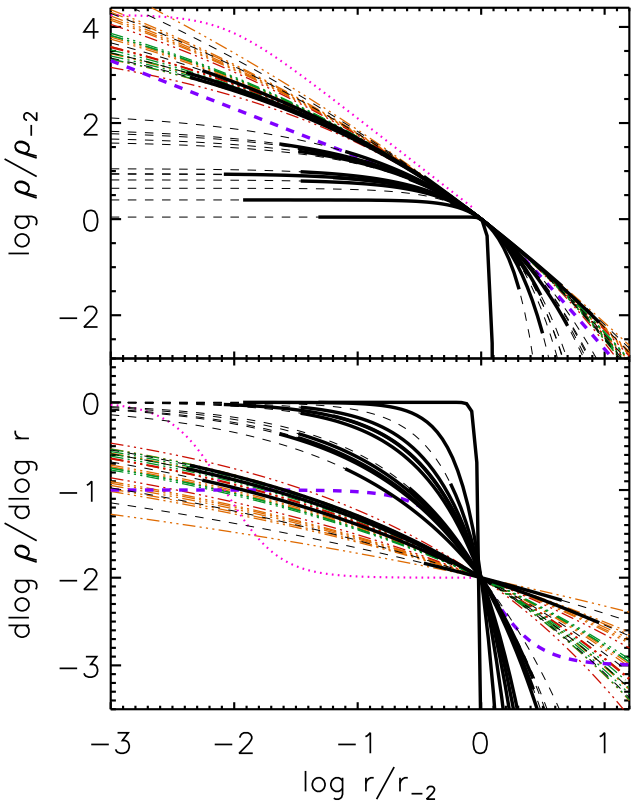

FIG. 9.— Dark matter density profiles (*top*) and density slope profiles (*bottom*) for the fit Einasto halos (*black, solid lines*). Only results for the Kroupa IMF are shown for clarity. For each halo the radial range of the observations is highlighted by a thick line. Colored dashed-dotted lines represent Einasto halos from ΛCDM simulations whose parameters are shown in Fig. 6. A purple dashed line represents a generic galaxy-sized NFW halo, a magenta dotted line a generic galaxy-sized Iso halo.

As a reminder, an almost constant dark matter density has been found for a large sample of dark matter dominated galaxies (e.g. de Blok & Bosma 2002). These authors have found a mean inner density slope $\alpha \sim -0.2$, as measured "directly" from optical spectroscopy by inverting the RCs into volume densities and extracting the slope at the innermost data point of the observations. We do not know yet the average slope that would be fit with the Einasto profile for similar low surface brightness objects. The current THINGS sample consists mostly of galaxies more massive than those in de Blok & Bosma (2002) (stellar and total masses), despite the presence of a few low surface density objects (among which NGC 2366 is common with de Blok & Bosma 2002). Note, however, that both samples show comparable average inner density slopes of dark matter. At first it may seem surprising because the quantity of baryons strongly differs in those samples. That particularity will be investigated in a future paper of our series.

5.3. *Halo concentration versus Einasto index and mass*

We have derived the virial radius r_{200} and halo concentration $c_{200} = r_{200}/r_{-2}$ as the radius of a sphere of mean density ρ_{200} which equals two hundred times the critical density for closure of the Universe, $\rho_{\rm crit} = 3H_0^2/8\pi G$. We derive the (halo) mass M_{200} at r_{200} using Eq. 4. Figure 10 compares the virial masses, halo concentrations and indices. Concentrations and virial masses are reported in Tab. 4. For clarity, the fourth halo family has been omitted in Fig. 10 and Tab. 4.

Adopting the Kroupa stellar mass scaling, it is observed that the Einasto index increases with the halo mass for halos more massive than $M_{200} \sim 2 \times 10^{11}\ h^{-1}\ \mathcal{M}_\odot$ while its distribution is more scattered for less massive halos, showing an almost flat part. That curved trend is less evident with the diet-Salpeter IMF results. Though the mass range spanned by the observations is relatively small in comparison to what can be probed by numerical models, the complex relation between Einasto index and mass illustrates that no "universal" galactic dark matter halo can be identified from these observations: the Einasto index cannot be simply deduced from the halo mass, nor does a simple scaling law allows one to scale the Einasto index/mass profile to those of a halo with a different mass. Our observational result thus confirms the non-universality of Einasto halos seen in numerical simulations (Navarro et al. 2010).

The concentration is not correlated with the Einasto index (right-hand panel), but tends to decrease with the mass (middle panel). The scatter of the trend is however significant. Halo fits with the diet-Salpeter IMF are less concentrated than halo fits with the Kroupa IMF, as caused by the more important contribution of the stellar component. As a comparison, the expected dependencies of the Einasto and NFW concentrations on the halo virial mass from cosmological simulations (Neto et al. 2007; Macciò et al. 2008; Gao et al. 2008) are displayed as well. These authors have found concentrations basically scaling with the total mass as $c_{200} \propto M_{200}^{-0.1}$. If one omits the two outliers which are the most concentrated and cuspiest halos, the relations of Neto et al. (2007) and Gao et al. (2008) are in good agreement with the seven halos at the upper end of the $c_{200} - M_{200}$ trend for the Kroupa IMF, and thus above most of concentrations derived with the diet-Salpeter IMF. The NFW relation of Macciò et al. (2008) is more consistent with the lower end of the remaining halos at the lower end of the concentrations. Notice however that the comparison is of limited value as the halo masses can be measured directly from the numerical simulations whereas we can only provide estimates for the observations.

We finally note that possible correlations between the properties of the Einasto halos with those of the baryonic matter (absolute magnitude, baryonic gas masses, disk and bulge characteristic scalelengths, etc.) will be fully studied into a forthcoming paper of our series (Chemin et al., in preparation). A preliminary analysis nevertheless shows Einasto indices scaling with (total) stellar masses, but barely with e.g. the bulge-to-disk luminosity ratio.

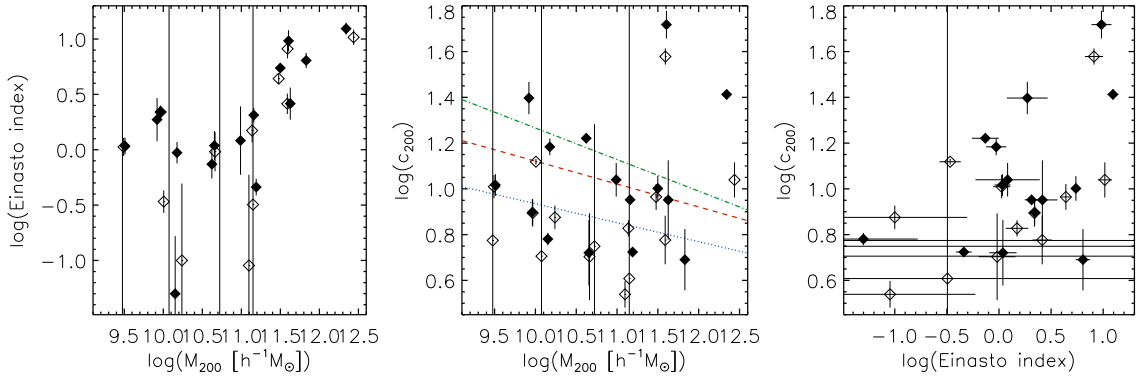

FIG. 10.— Virial masses M_{200}, concentrations c_{200} and indices of Einasto halos. Open (filled) symbols are for the diet-Salpeter (Kroupa, respectively) IMF. In the middle panel a green dashed-dotted line represents the dependency of the Einasto halo concentrations on the mass $\log(c_{200}) = 2.646 - 0.138\log(M_{200})$ from numerical simulations (Gao et al. 2008, concentrations derived with fixed Einasto indices), a blue dotted the dependency of the NFW halo concentrations $\log(c_{200}) = 1.765 - 0.083\log(M_{200})$ (Macciò et al. 2008) and a red dashed line the dependency of the NFW halo concentrations $\log(c_{200}) = 2.121 - 0.1\log(M_{200})$ (Neto et al. 2007). Halos with $\log(n) \sim -3$ are not displayed for clarity reasons.

5.4. *The influence of total gas densities on Einasto parameters*

The contribution of the molecular gas has been neglected in our study. This is justified since the total gas surface densities are dominated by those of the atomic gas for most of the sample. Even when molecules dominate the total gas density in the innermost regions of a few galaxies from our sample (NGC 3521, NGC 4736, NGC 5055, NGC 6946; Leroy et al. 2008), the stellar surface densities completely dominate the mass budget of the baryons in those regions. They are generally more than ten times larger than the molecular densities, with the exception of NGC 6946 where the ratio of the surface density of molecules to that of the stars sometimes reaches a factor of 1/3 in its central kiloparsec (Leroy et al. 2008).[7] We have thus fit Einasto models by adding the molecular gas component to the mass distribution for NGC 6946 only, with H_2 surface densities from Leroy et al. (2008). The top panel of Fig. 11 shows the results of that mass distribution model. As a result, the quality of fit remains unchanged with the Kroupa IMF ($\chi^2_r \sim 1.0$), as well as ρ_{-2} and r_{-2} within the uncertainties, with $\rho_{-2} = (2.7 \pm 1.0) \times 10^{-3}$ $\mathcal{M}_\odot$ pc^{-3} and $r_{-2} = (15.9 \pm 3.7)$ kpc. The Einasto index becomes $n = 1.2 \pm 0.4$, which is about half the value derived with no molecular gas ($n = 2.6 \pm 0.9$). Such a difference of halo cuspiness is clearly seen in the bottom panel of Fig. 11 (green curve), where the difference of the Einasto halo RCs reach 20 km s^{-1} at 3 kpc. Though NGC 6946 is probably an extreme case where the influence of the molecular gas is maximum on the halo shape, it is likely that Einasto indices would be even lower had we included the molecules in our fits. We also think the total gas component could play a more important contribution to the total baryonic dynamical budget than in our current study if models were done under the assumption of *free* stellar mass-to-light ratios. However such an hypothesis of $\Upsilon_{3.6\mu m}$ is beyond the scope of the article and we defer a complete analysis of the influence of the total/molecular gas contribution onto Einasto models with free mass-to-light ratios to our forthcoming article (Chemin et al., in preparation).

[7] Since the stellar masses we use are larger than those given by Leroy et al. (2008), as explained in D08, that ratio of molecular gas to stellar surface densities is even smaller in our current analysis than in Leroy et al. (2008).

6. STRENGTHS AND WEAKNESSES OF EINASTO ΛCDM HALOS

We now compare more precisely the parameter space of observed Einasto halos with those derived from

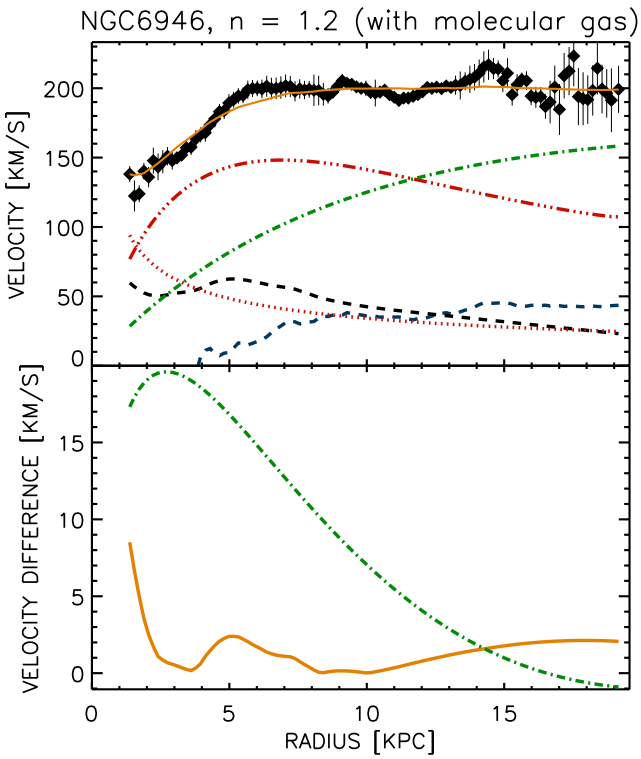

FIG. 11.— Mass model of NGC 6946 with the molecular gas contribution *(*top panel). The molecular gas RC is shown by a black dashed line. All other stellar and gas curves are from Fig. 4. The bottom panel displays the differences between RCs of the total models of NGC 6946 done with and without the molecular gas (orange solid line, in absolute values), and between the corresponding Einasto halo RCs (green dashed-dotted line).

TABLE 4
EINASTO HALO CONCENTRATION c_{200} AND VIRIAL MASS M_{200}

Galaxy	$\log(c_{200})$ (1)	$\sigma_{\log}$ (2)	$\log(M_{200})$ (3)	$\log(c_{200})$ (4)	$\sigma_{\log}$ (5)	$\log(M_{200})$ (6)
NGC925	0.71	46.9	10.07	0.78	0.03	10.15
NGC2366	1.01	0.05	9.49	1.02	0.05	9.51
NGC2403	0.96	0.06	11.48	1.00	0.05	11.50
NGC2841	1.04	0.08	12.44	1.41	0.02	12.34
NGC2903	1.58	0.04	11.59	1.72	0.06	11.61
NGC3031	0.88	0.05	10.24	1.22	0.02	10.62
NGC3198	0.83	0.04	11.14	0.95	0.02	11.16
IC2574	0.70	0.19	10.66	0.72	0.14	10.66
NGC3521	0.61	1.73	11.15	1.04	0.07	10.99
NGC3621	0.78	0.11	11.59	0.69	0.13	11.83
NGC4736	0.77	1.35	9.48	1.40	0.07	9.92
DDO154	0.89	0.06	9.97	0.90	0.06	9.96
NGC5055	0.54	0.06	11.10	0.72	0.14	11.19
NGC6946	0.75	0.53	10.72	0.95	0.02	11.63
NGC7793	1.12	0.01	10.00	1.18	0.04	10.18

NOTE. — Columns (1)-(2)-(3) are for the diet-Salpeter IMF and (4)-(5)-(6) for the Kroupa IMF. $\sigma_{\log}$ is the $1\sigma-$error on $\log(c_{200})$. M_{200} is in $h^{-1}\ \mathcal{M}_{\odot}$.

ΛCDM dissipationless simulations (e.g. Navarro et al. 2004, 2010).

A first caveat to this comparison is that, despite the wide global range of halo masses explored in these simulations, the halo masses do not span the whole range of our galaxies, namely $10^{9.5-12.5}\ h^{-1}M_{\odot}$. A larger mass range of simulated galaxy-sized halos is required for future comparisons with observations.

Secondly, and more importantly, these simulations usually ignore the gaseous component of galaxies, whose dissipative nature leads them to concentrate in the cores of halos and possibly force the dark matter to respond to the concentration of the dominant central baryons. For this reason, we have also compared our results with those from Tissera et al. (2010) who have included the physics of baryons in the galactic halos of the Aquarius simulations (Springel et al. 2008) by means of hydrodynamical models.

Finally, the innermost regions of galactic halos are still hardly resolved by cosmological numerical simulations (at scales $r < r_{200}/1000$), as noted in, e.g., Navarro et al. (2010).

We distinguish here between fits performed with a free index and fits done with a fixed index in order to investigate whether the typical Einasto index seen in ΛCDM simulations matches the observations. We have thus performed fits with a fixed index $n = 6.2$, which is the average value of galaxy-sized halos presented in Navarro et al. (2004).

6.1. *Models with a free index*

Figures 6 and 7 show that most of the observed and simulated galaxy-sized halos share the same characteristic scale densities and radii but not their indices. The indices of half of our observed halos are usually less than half the mean value of the simulated ones (i.e. $n < 3$). The Einasto indices for baryons+dark matter simulations from Tissera et al. (2010) differ even more from our observations than do the pure dark matter halo indices. The addition of hydrodynamics in the ΛCDM simulations drags more dark matter towards the centre of halos, as likely caused by gas dissipational effects, thus pushing the index towards larger values ($n \to 10$) than for the pure dark matter case ($n \sim 6$), while the observations go to an opposite way ($n \to 1-2$). Note though recent hydrodynamical cosmological simulations by Governato et al. (2010) with strong SN feedback coupled with a high threshold for star formation lead to dark matter halos without cusps. As theoretically explained by Pontzen & Governato (2011), episodic SN events in dwarf galaxies alter the dark matter distribution in non-adiabatic ways leading to cored profiles.

Only a few galaxies have a parameter space in rough agreement with simulations within the quoted uncertainties, though with some subtle differences. For instance, NGC 2903 can be associated with a dwarf-sized simulated halo in the index-radius graph, but with a halo more massive than that of a dwarf galaxy ($\log(\rho_{-2}) \sim -1$ $\mathcal{M}_{\odot}$ pc^{-3}) in the index-density parameter space. For NGC 3621 any (dis)agreement depends critically on the chosen IMF. Only NGC 2841 and NGC 2403 seem to be galaxies whose halo parameters are in full agreement with cuspy ΛCDM Einasto halos.

Another interesting point concerns the results for the few dwarf and low surface brightness galaxies DDO 154 and NGC 2366. Due to their dark matter dominance they are ideal candidates for a direct comparison with ΛCDM low mass halos ($10^9\ h^{-1}\ \mathcal{M}_{\odot}$). They perfectly agree with simulated dwarf galaxy halos in the density-radius parameter space (the two closest symbols to the red triangles in Figs 6 and 7) but they have a low Einasto index, contrary to all simulated dwarf-galaxy-sized halos.

6.2. *Cuspy Einasto models with a fixed index*

We now investigate whether Einasto halos with an index close to the typical index seen in cosmological simulations agree better with the observations than the NFW and Iso halos. The HI RCs have therefore been fit with a Einasto fixed value ($n = 6.2$) model. These fits have two free parameters, like the NFW and core halos. The results for both IMFs are reported in Tab. 5 and the RC decompositions are displayed in Fig. 12 (Kroupa IMF only). Figure 13 compares the quality of fits between the fixed Einasto index models to the free Einasto index models (left-hand panel), and to the NFW and Iso models (right-hand panel), whereas Figure 14 displays the parameter space $[\rho_{-2}, r_{-2}]$ obtained for $n = 6.2$.

As seen in Fig. 13, the fits performed with a fixed index $n = 6.2$ are significantly worse than those with a free index, regardless of the IMF (84% and 89% of our sample for the diet-Salpeter and Kroupa IMFs, respectively). They also provide worse results than the Iso model, regardless of the IMF (65% and 55% for the diet-Salpeter and Kroupa IMFs, respectively), and better results than the NFW model fits, regardless of the IMF (75% and 80% for the diet-Salpeter and Kroupa IMFs, respectively).

The parameter space of the characteristic scale densities and radii still shows a correlation (Fig. 14), but with more scatter than seen in Figs. 6 and 7 for fits done with a free index. The striking feature is the larger range of densities and radii than for the fits performed with free indices. The relation between r_{-2} and $\rho(r_{-2})$ is steeper than the previous one given in §5.1 and Fig. 7. Besides the fact that extreme halos of low density and large extent appear unrealistic for galaxies, the agreement with the expected galaxy-size range seen in cosmological sim-

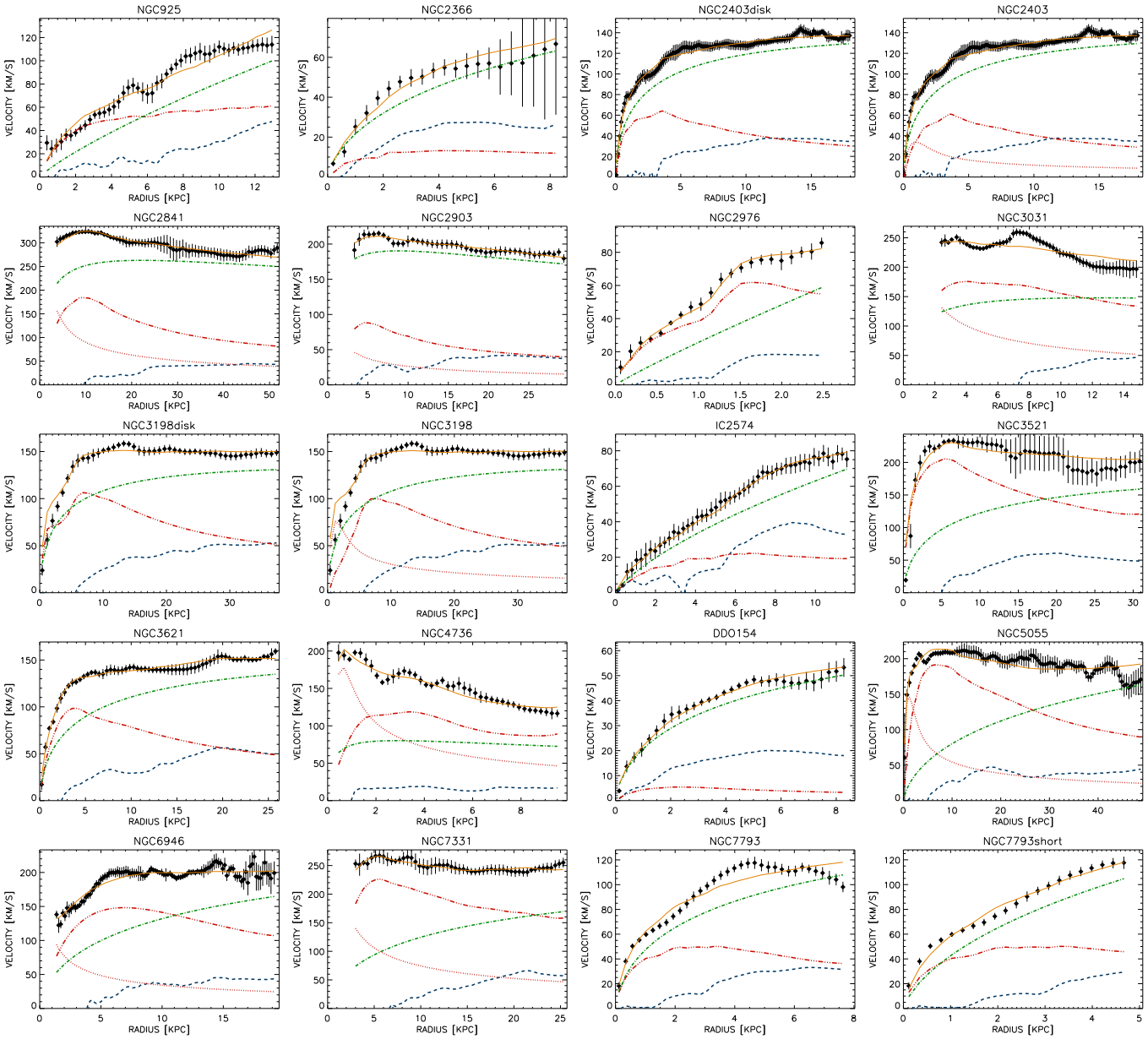

FIG. 12.— Same as Fig. 4 but with a fixed index $n = 6.2$.

ulations becomes worse and several fit halos exceed the cluster-sized regime. We therefore conclude that Einasto halos with a fixed index $n \sim 6$ are ruled out by the analysis of RCs of galaxies.

7. TWO-PARAMETER EINASTO MODELS

In the previous section we have studied two-parameter, fixed index Einasto halos that were consistent with CDM, but noted they were not consistent with the observations. In this section, we try to identify other two-parameter Einasto halos and ask whether there are any Einasto models that can describe the observed halos better than the Iso or NFW halo models. Before answering these questions, we emphasize that our galaxy sample does not pretend to be representative of the whole diversity of spiral galaxies in the local Universe. Nevertheless, in this section, we aim at finding a family of generic Einasto halos that reproduce fairly well the RCs of THINGS spiral galaxies, at least as good as the usual core or cosmological cuspy models.

7.1. *Cuspy Einasto halos versus the NFW halo*

We estimate the critical index value where the NFW halo becomes better than the Einasto halo for the majority of the current sample. We find $n_{\rm up} \sim 10 - 11$ for the diet-Salpeter IMF and $n_{\rm up} \sim 11 - 12$ for the Kroupa IMF. Those values have been derived by increasing progressively the (fixed) index in the fits and by identifying the turnover index where more than half of the NFW fits from the sample becomes better than the Einasto fits. Note that those models represent halos which are less and less dense, and larger as the index increases. Another advantage of these models with respect to the NFW model is the better agreement with ΛCDM simu-

TABLE 5
FIT PARAMETERS OF THE EINASTO HALO TO THINGS GALAXIES FOR A FIXED INDEX $n = 6.2$ AND MASS-TO-LIGHT RATIOS DERIVED USING A DIET-SALPETER (LEFT PANEL) AND KROUPA (RIGHT PANEL) IMFS.

Galaxy	diet-Salpeter			Kroupa		
	χ^2_r	ρ_{-2} (10^{-3} $\mathcal{M}_\odot$ pc^{-3})	r_{-2} (kpc)	χ^2_r	ρ_{-2} (10^{-3} $\mathcal{M}_\odot$ pc^{-3})	r_{-2} (kpc)
NGC925	2.2	$1.2\times10^{-5} \pm 8.0\times10^{-7}$	> 1000	1.4	$1.8\times10^{-4} \pm 1.5\times10^{-4}$	$1.6\times10^{5} \pm 3.3\times10^{5}$
NGC2366	0.6	$1.8\times10^{-2} \pm 8.9\times10^{-3}$	159.0 ± 80.9	0.6	$2.0\times10^{-2} \pm 9.5\times10^{-3}$	150.0 ± 73.8
NGC2403d	0.6	$5.8\times10^{-1} \pm 5.0\times10^{-2}$	26.7 ± 1.5	0.6	$1.2 \pm 8.7\times10^{-2}$	17.8 ± 0.8
NGC2403	0.6	$5.5\times10^{-1} \pm 4.9\times10^{-2}$	27.7 ± 1.6	0.6	$1.1 \pm 8.5\times10^{-2}$	18.2 ± 0.8
NGC2841	0.3	$3.6 \pm 2.1\times10^{-1}$	18.9 ± 0.6	0.3	$14.3 \pm 7.7\times10^{-1}$	10.0 ± 0.3
NGC2903	0.3	31.6 ± 2.5	4.7 ± 0.2	0.3	48.1 ± 3.9	3.9 ± 0.1
NGC2976	2.0	$4.7\times10^{-5} \pm 1.3\times10^{-5}$	> 1000	0.5	$4.2\times10^{-4} \pm 3.5\times10^{-4}$	$3.6\times10^{6} \pm 1.7\times10^{7}$
NGC3031	4.3	$1.2\times10^{-2} \pm 2.2\times10^{-2}$	417.0 ± 760.0	3.7	14.4 ± 7.3	5.6 ± 1.5
NGC3198d	1.9	$1.1\times10^{-1} \pm 3.6\times10^{-2}$	62.9 ± 13.6	1.8	$5.3\times10^{-1} \pm 1.3\times10^{-1}$	26.1 ± 3.6
NGC3198	3.2	$9.7\times10^{-2} \pm 4.2\times10^{-2}$	66.9 ± 18.9	2.6	$4.9\times10^{-1} \pm 1.5\times10^{-1}$	27.2 ± 4.7
IC2574	0.3	$2.4\times10^{-4} \pm 8.0\times10^{-5}$	> 1000	0.3	$4.5\times10^{-4} \pm 1.3\times10^{-4}$	9170 ± 4520
NGC3521	8.3	$4.2\times10^{-6} \pm 1.5\times10^{-6}$	> 1000	5.7	$2.6\times10^{-1} \pm 2.7\times10^{-1}$	50.3 ± 36.7
NGC3621	0.8	$3.9\times10^{-2} \pm 6.7\times10^{-3}$	147.0 ± 19.4	0.5	$3.2\times10^{-1} \pm 3.1\times10^{-2}$	37.6 ± 2.3
NGC4736	1.6	$3.3\times10^{-1} \pm 1.1$	12.1 ± 24.8	1.6	78.8 ± 52.2	1.3 ± 0.4
DDO154	0.8	$4.4\times10^{-2} \pm 1.2\times10^{-2}$	54.1 ± 11.8	0.8	$4.6\times10^{-2} \pm 1.2\times10^{-2}$	52.3 ± 11.4
NGC5055	8.3	$3.7\times10^{-6} \pm 3.2\times10^{-7}$	> 1000	1.5	$6.7\times10^{-3} \pm 2.6\times10^{-3}$	541.0 ± 182.0
NGC6946	1.5	$6.2\times10^{-5} \pm 5.0\times10^{-5}$	> 1000	1.0	$1.1\times10^{-1} \pm 2.9\times10^{-2}$	106.0 ± 21.8
NGC7331	3.0	$6.4\times10^{-6} \pm 6.7\times10^{-7}$	> 1000	0.3	$9.2\times10^{-2} \pm 2.7\times10^{-2}$	112.0 ± 24.4
NGC7793	4.1	$1.1\times10^{-1} \pm 5.3\times10^{-2}$	89.2 ± 39.1	3.9	$2.9\times10^{-1} \pm 1.1\times10^{-1}$	42.8 ± 13.2
NGC7793s	1.5	$5.4\times10^{-3} \pm 3.0\times10^{-3}$	> 1000	1.8	$4.1\times10^{-2} \pm 1.8\times10^{-2}$	324.0 ± 162.0

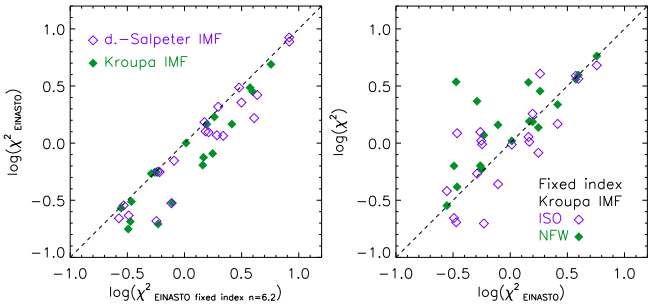

FIG. 13.— Comparison of reduced χ^2 for Einasto halo models done at fixed index ($n = 6.2$) with Einasto halo models done at free index (*left*). Open and filled symbols are for the diet-Salpeter and Kroupa IMFs, respectively. Comparison of reduced χ^2 for $n = 6.2$ Einasto halo models with the NFW and Iso halos (respectively filled and open symbols) with the Kroupa IMF (*right*). See Tab. 5 for results obtained with the diet-Salpeter IMF.

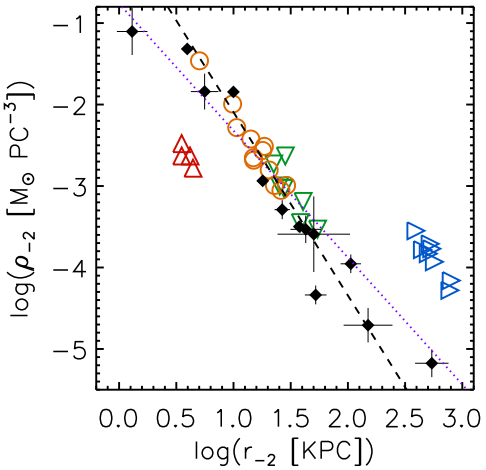

FIG. 14.— Parameter space of Einasto halos with a fixed index ($n = 6.2$) for the Kroupa IMF. See Tab. 5 for results obtained with the diet-Salpeter IMF. Results for the few halos having an extremely large scale radius are not shown for clarity. Colored symbols correspond to the same cosmological halos as in Figs. 6 and 7. Additional blue, open triangles correspond to simulated cluster-sized halos from Navarro et al. (2004). A dashed line is a power law fit to the relationship $\log(\rho_{-2}) = (-2.25 \pm 0.04)\log(r_{-2}) + (0.16 \pm 0.05)$. As a comparison, a dotted line represents the linear fit to the relationship obtained from Einasto models done at free Einasto index (see §5.1 and Fig. 7).

lations.

We repeat the same procedure but towards smaller indices and find $n_{\rm low} \sim 0.5$ (diet-Salpeter IMF) and $n_{\rm low} \sim 1$ (Kroupa IMF) as the values where the majority of constrained Einasto fits turn better than NFW ones. This result is completely expected because small indices provide core halos, whose halo shape is naturally better for the sample than any cusp.

7.2. *Core Einasto halos versus the pseudo-isothermal sphere*

In contrast with the cuspy halos, we find the cored ($n < 4$) halos at the low end of the Einasto index distribution. We investigate the goodness of fit of two-parameter Einasto models performed with a fixed, small index to find a critical index where the majority of such constrained Einasto fits become worse than those performed with the Iso model. It turns out a low limit cannot be obtained for the diet-Salpeter IMF; the Iso model is always a better fit than the constrained Einasto model at a level of ∼70%, which is likely explained by the relatively scattered index distribution, as seen in §5.1. In other words it is almost impossible to find an index that would satisfy most of all halos at the same time for that IMF. It is not the case for the Kroupa IMF for which $n_{\rm low} \sim 2$ indicates the turnover index. Indeed, 65%, 55% and 45% of all the sample is better fit by the Iso model than $n = 1$, $n = 2$ and $n = 3$ (respectively) Einasto fits. Notice this value appears consistent with the mean index

$\bar{n} = 1.4 \pm 0.8$ of non-cuspy halos fit under the Kroupa IMF assumption (§5.1).

For larger indices $n_{\rm up} \sim 5$ is the limit where most of constrained Einasto fits become worse than Iso ones. Past this value, the core nature of the Iso model starts to dominate the cuspy nature of these Einasto halos. The index range $2 \leq n \leq 4$ of constrained Einasto core models is therefore small compared with that of constrained Einasto cusps.

7.3. *Towards a new two-parameter density profile*

Both results of §7.1 and §7.2 make us conclude that the family of two-parameter Einasto models with $4 < n \leq 12$ is more suited for the modeling of observational cuspy halos than is the NFW model, whereas the Einasto model with $2 \leq n \leq 4$ is more suited for the modeling of cored halos than is the isothermal model. While allowing the variation of the Einasto index is essential in finding the best fit models to the THINGS RCs (§4, §5 and §6), those fits at fixed indices point out the exponential shape of the density profile also contributes in better modeling the mass distribution of the galaxies. We thus suggest that a new shape of dark matter density, where the volumic density profile decreases exponentially as a function of radius following Eq. 3, may be a good alternative to the usual mass divergent, pseudo-isothermal and NFW models, with Einasto indices chosen to match the particular type of halo (core or cusp) one wants to model.

8. CONCLUSIONS

For the first time, the Einasto dark matter halo has been applied to model the mass distribution of nearby and undisturbed galactic disks. Our results show that the Einasto model is a good fit of the dark matter contribution to highly-resolved HI rotation curves of galaxies, better than other models like the (cored) Iso model or the (cuspy) NFW model. The significant improvement is caused by the parameter that shapes the radial behaviour of the mass density profile, the Einasto index. The big advantage of the Einasto formalism over the NFW cusp or the pseudo-isothermal sphere lies on its third parameter, the index, which allows for extra freedom in describing different shapes of density profiles. The larger (respectively, smaller) is the Einasto index, the cuspier (shallower) is the halo in its central parts. Since there is no unique index describing all halos, it is not possible to scale the density profile from one galaxy to another with a different mass. In other words, we find no evidence for a universal dark matter Einasto halo, at least in the galaxy sample we have analyzed. This result corroborates the one found in dissipationless ΛCDM simulations. Noteworthy however is the fact that the index appears to scale with the halo mass for halos more massive than $M_{200} \sim 2 \times 10^{11}\ h^{-1}\ \mathcal{M}_{\odot}$.

We find that the Einasto index is generally smaller than the one inferred from cosmological simulations, by a factor of two or more. This discrepancy between observed and simulated Einasto indices extends the core-cusp controversy (Iso versus NFW) to the Einasto formalism. A ΛCDM Einasto halo is cuspier than an observed galactic Einasto halo. In our sample, galaxies with a cuspy (i.e. with $n > 4$) Einasto halo are not frequent. It is interesting to note that our sample consists of both normal, bright galaxies and of a few dwarf, low surface density galaxies, while the cusp-core controversy usually deals with small and low surface density galaxies only. Cored dark matter halos are thus found in galaxies whose baryonic content significantly differs, for halos less massive than $M_{200} \sim 2 \times 10^{11}\ h^{-1}\ \mathcal{M}_{\odot}$.

The RC decomposition has also shown that cuspy Einasto halos with fixed index $4 < n \leq 12$ give a better description of RCs than does the NFW model. Conversely core Einasto models with fixed index $2 \leq n \leq 4$ give better RC fits than the Iso model. It implies that the exponential decrease of the Einasto dark matter density is also responsible for the improvement in modeling the mass distribution of galaxies, in addition to the effect of the Einasto index. Those constrained Einasto models can be a good alternative to Iso or NFW models for galactic dynamics, but we re-iterate here that Einasto models with free index are preferable over any of those two-parameter models.

The analysis has shown that the stellar masses derived with the Bell & de Jong (2001) prescription under a diet-Salpeter IMF hypothesis are in conflict with the Einasto model. This is not the case for the Kroupa IMF. In future papers from this series, we will perform mass models with free stellar masses and with other fixed stellar mass scalings, like the one described in Chabrier (2003). Additional improvements of dynamical models will take into account the molecular gas content, where available.

Furthermore we will investigate possible correlations between the properties of Einasto dark matter halos and baryons. The mass distribution for a large sample of low surface density disks will also be studied. We expect that those galaxies exhibit low Einasto indices because of the shallow nature of the density profile in their core, but to which extent their values compare with those of normal, higher surface brightness disks like most of our current THINGS subsample is not known yet. Both these samples will help us to measure the variation of dark halo inner shape as a function of galaxy mass.

We finally emphasize the importance of testing the Einasto halo model for objects at extreme ends of the galaxy luminosity function (dwarf spheroidals and giant ellipticals). This will be crucial for getting a complete description of the observational behaviour of Einasto models over several decades of halo mass and comparing with expectations from ΛCDM simulations at similar cosmological scales.

We are very grateful to the referee, Matt Bershady, for helpful comments and suggestions. Laurent Chemin acknowledges financial support from RadioNet-FP7 and Région Aquitaine. The work of WJGdB is based upon research supported by the South African Research Chairs Initiative of the Department of Science and Technology and National Research Foundation.

REFERENCES

Akaike, H., 1974, IEEE Trans. Automatic Control, 19, 716
Barnes, E. I., Sellwood, J. A., Kosowsky, A., 2004, AJ, 128, 2724
Bell, E. F., & de Jong, R. S., 2001, ApJ, 550, 212

Cardone, V.F., Piedipalumbo, E., & Tortora, C. 2005, MNRAS, 358, 1325
Chabrier, G., 2003, PASP, 115, 763
Chemin, L., Carignan, C. & Foster, T. 2009, ApJ, 705, 1395
de Blok, W. J. G., & Bosma, A. 2002, A&A, 385, 816
de Blok, W. J. G., 2004, IAU Symp. 220, Dark Matter in Galaxies, eds. S. D. Ryder et al. (San Francisco: ASP), 69
de Blok, W. J. G., Walter, F., Brinks, E., Trachternach, C., Oh, S.-H., & Kennicutt, R. C., 2008, AJ, 136, 2648
Diemand, J., Moore, B., Stadel, J., 2004, MNRAS, 353, 624
Donato, F., Gentile, G., Salucci, P., Frigerio Martins, C., Wilkinson, M. I., Gilmore, G., Grebel, E. K., Koch, A., et al., 2009, MNRAS, 397, 1169
Einasto, J., 1965, Trudy Inst. Astrofiz. Alma-Ata, 51, 87
Einasto, J., 1968, PTarO, 36, 414
Einasto, J., 1969, Astronomische Nachrichten 291, 97
Gao, L., Navarro, J. F., Cole S., Frenk, C. S., White, S. D. M., Springel, V., Jenkins, A., Neto, A. F., 2008, MNRAS, 387, 536
Governato, F., Brook, C., Mayer, L., Brooks, A., Rhee, G., Wadsley, J., Jonsson, P., Willman, B., et al., 2010, Nature, 463, 203
Graham, A. W., Merritt, D., Moore, B., Diemand, J., & Terzić, B., 2006, AJ, 132, 2701
Jing, Y. P., & Suto, Y., 2000, ApJ, 529, L69
Kennicutt, R. C., et al. 2003, PASP, 115, 928
Kormendy, J., & Freeman, K. C., 2004, IAU Symp. 220, Dark Matter in Galaxies, eds. S. D. Ryder et al. (San Francisco: ASP), 377
Kormendy, J., Fisher, D. B., Cornell, M. E., Bender, R., 2009, ApJS, 182, 216
Kregel, M., van der Kruit, P. C., & de Grijs, R. 2002, MNRAS, 334, 646
Kroupa, P., 2001, MNRAS, 322, 231
Kuzio de Naray, R., McGaugh, S. S., de Blok, W. J. G., & Bosma, A., 2006, ApJS, 165, 461
Kuzio de Naray, R., McGaugh, S. S., & de Blok, W. J. G., 2008, ApJ, 676, 920
Leroy, A. K., Walter, F., Brinks, E., Bigiel, F., de Blok, W. J. G., Madore, B., & Thornley, M. D., 2008, AJ, 136, 2782
Łokas, E. L., & Mamon, G. A., 2001, MNRAS, 321, 155
Macciò, A. V., Dutton, A. A., & van den Bosch, F. C., 2008, MNRAS, 391, 1940
Mamon, G.A., & Łokas, E.L. 2005, MNRAS, 362, 95
Merritt, D., Navarro, J. F., Ludlow, A., & Jenkins, A. 2005, ApJ, 624, 85
Merritt, D., Graham, A. W., Moore, B., Diemand, J., & Terzić, B. 2006, AJ, 132, 2685
Moore, B., Quinn, T., Governato, F., Stadel, J., Lake, G., 1999, MNRAS, 310, 1147
Navarro, J. F., Frenk, C. S., & White, S. D. M. 1996, ApJ, 462, 563
Navarro, J. F., Frenk, C. S., & White, S. D. M. 1997, ApJ, 490, 493
Navarro, J. F., Hayashi, E., Power, C., Jenkins, A. R., Frenk, C. S., White, S. D. M., Springel, V., Stadel, J., et al. 2004, MNRAS, 349, 1039
Navarro, J. F., Ludlow, A., Springel, V., Wang, J., Vogelsberger, M., White, S. D. M., Jenkins, A. R., Frenk, C. S., et al. 2010, MNRAS, 402, 21
Neto, A. F., Gao, L., Bett, P., Cole, S., Navarro, J. F., Frenk, C. S., White, S. D. M., Springel, V., et al., 2007, MNRAS, 381, 1450
Oh, S., de Blok, W. J. G., Walter, F., Brinks, E., & Kennicutt, R. C., 2008, AJ 136, 2761
Pontzen, A., & Governato, F., 2011, submitted to ApJ, arXiv:1106.0499
Sérsic, J.-L. 1968, Atlas de galaxias australes
Spano, M., Marcelin, M., Amram, P., Carignan, C., Épinat, B., & Hernandez, O., 2008, MNRAS, 383, 297
Spergel, D. N. et al. 2007, ApJS, 170, 377
Springel, V., Wang, J., Vogelsberger, M., Ludlow, A., Jenkins, A., Helmi, A., J. F. Navarro, J. F. N., Frenk, C. S., et al., MNRAS, 391, 1685
Stoehr, F., 2006, MNRAS, 365, 147
Tissera, P. B., White, S. D. M., Pedrosa, S., & Scannapieco, C., 2010, MNRAS, 406, 922
van der Kruit, P. C., & Searle, L. 1981, A&A, 95, 105
Walter, F., Brinks, E., de Blok, W. J. G., Bigiel, F., Kennicutt, R. C., Thornley, M. D., & Leroy, A. 2008, AJ, 136, 2563